Supplementary Information

Oriented tubular metal-organic framework superstructures via conjugate acid–base pair–mediated growth regulation

Giwook Lee,[a] *Sheng Chen,**[b] *Jongkook Hwang**[a c]

[a] Department of Energy Systems Research, Ajou University, 206 Worldcup-ro, Yeongtong-gu, Suwon 16499, Republic of Korea

[b] Key Laboratory for Soft Chemistry and Functional Materials, School of Chemistry and Chemical Engineering, School of Energy and Power Engineering, Nanjing University of Science and Technology, Ministry of Education, Nanjing, 210094, China

[c] Department of Chemical Engineering, Ajou University, 206 Worldcup-ro, Yeongtong-gu, Suwon 16499, Republic of Korea

Table of Contents

Section 1. Supplementary Figures

Section 2. Supplementary Tables

Section 1. Supplementary Figures

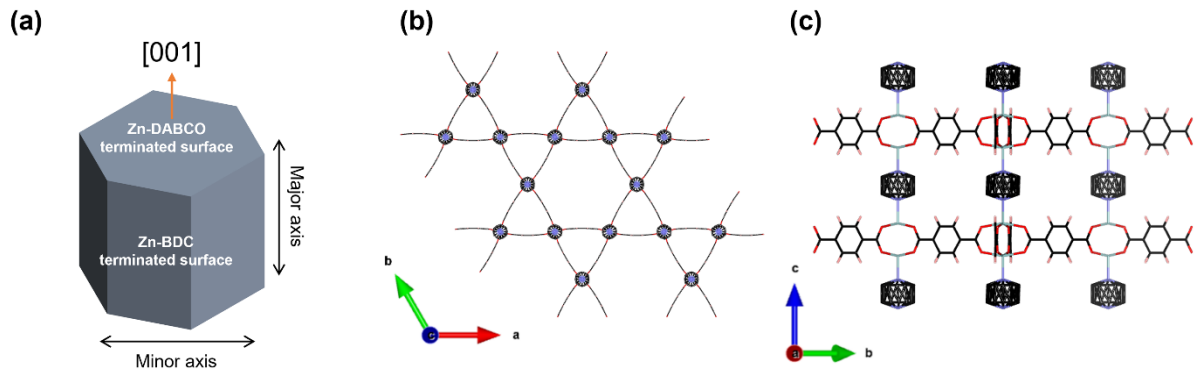

Fig. S1 Schematic illustration of ZnBD with Kagome crystal structure. Crystal formula $C_{22}H_{20}N_2O_8Zn_2$, M = 571.14, hexagonal, space group $P\bar{3}m1$ (No. 164), a = 21.620(1) Å, c = 9.628- (1) Å, V = 3897.3(5) Å^3, Z = 3, T = 173 K, ρ_{calcd} = 0.73 g/cm3, F(000) = 870, μ (Mo Kα) = 0.95 mm^{-1}, 2736 reflections observed [I > 2σ(I)]; R1 = 0.0520, wR2 = 0.1790.[S1]

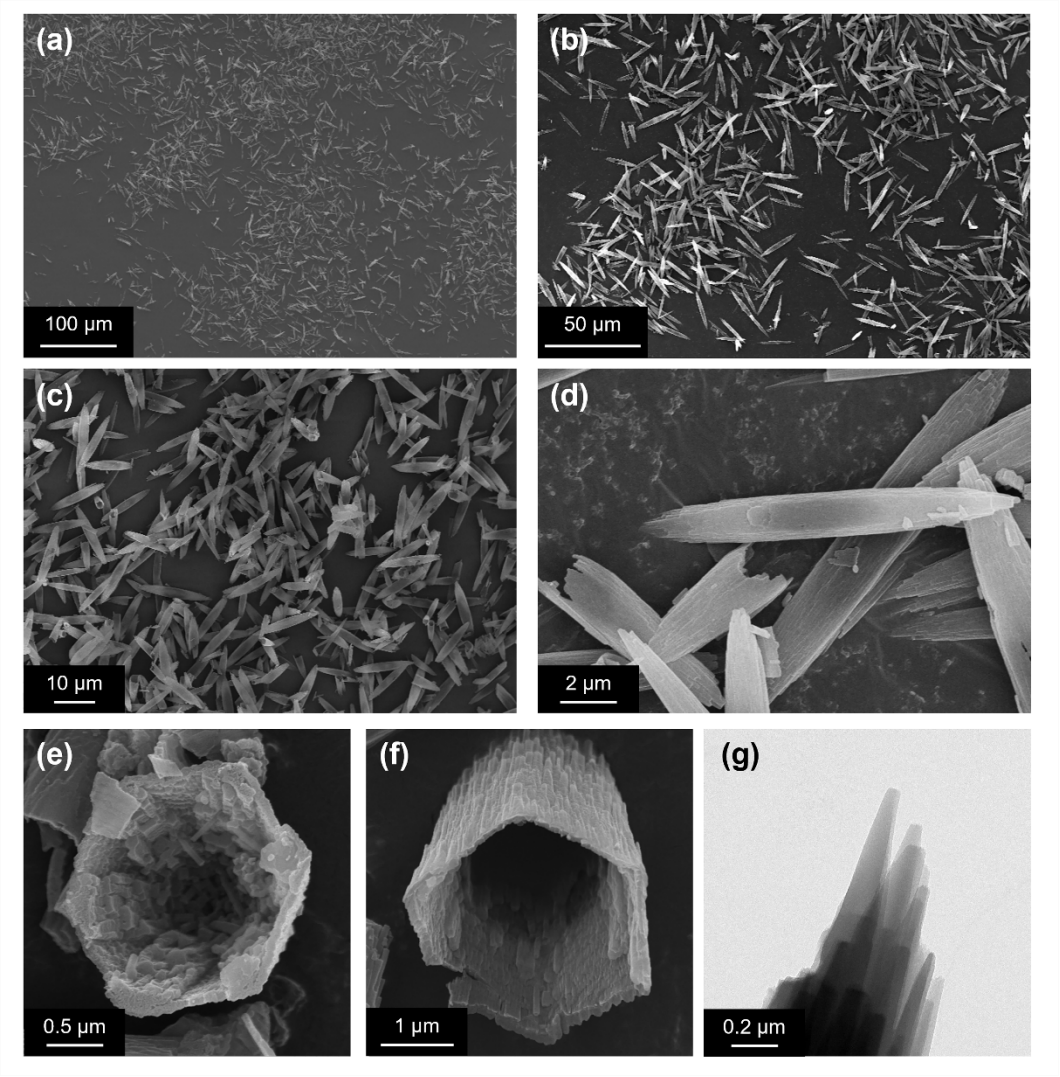

Fig. S2 SEM images at varying magnifications (a–d), cross-section (e, f) and TEM image (g) of OAc-AA-25.

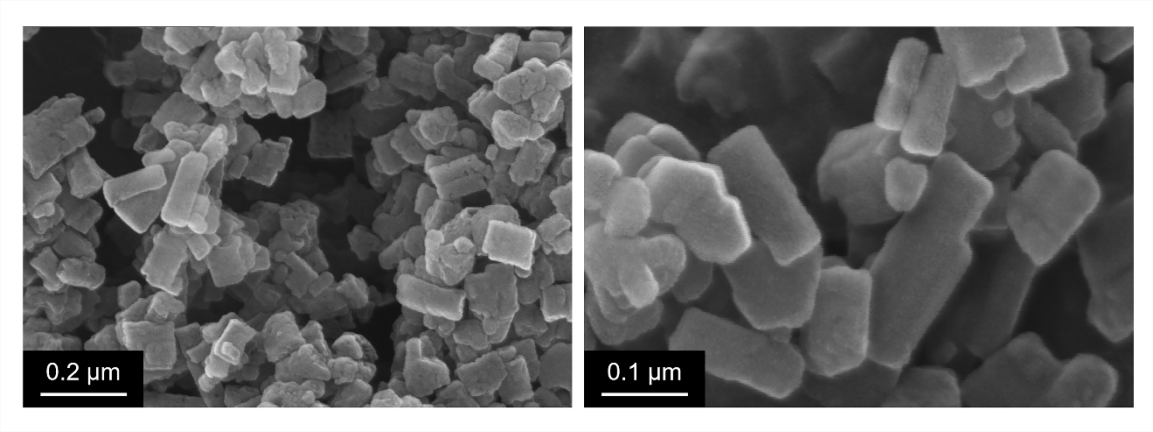

Fig. S3 SEM images at varying magnifications of OAc-AA-0.

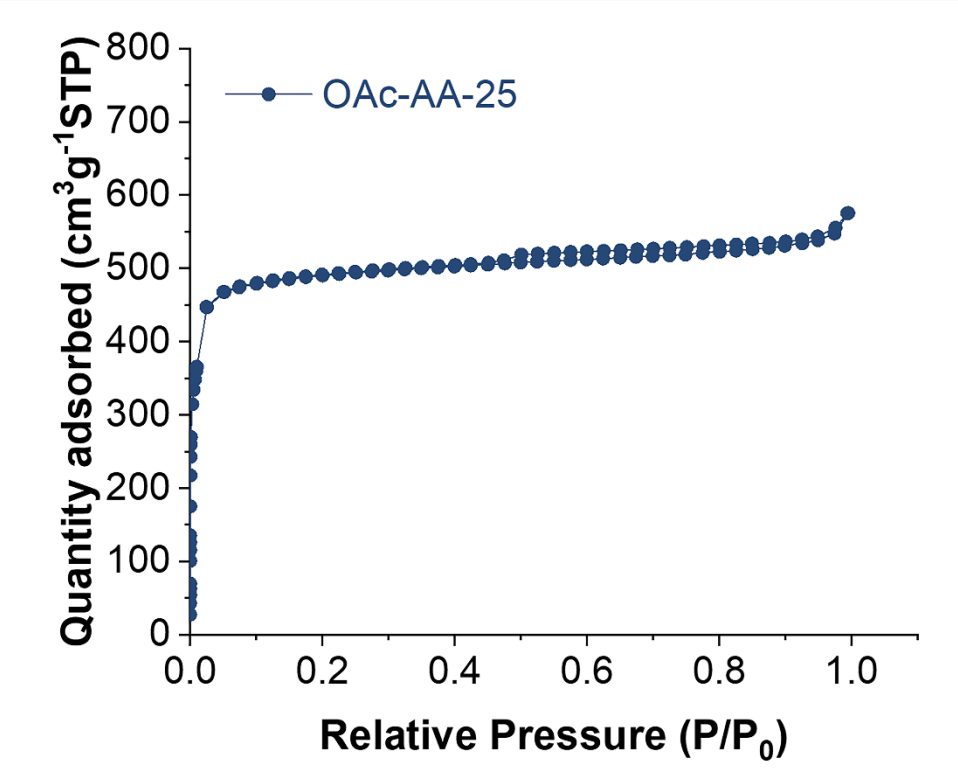

Fig. S4 N_2 sorption isotherm of OAc-AA-25 at 77 K.

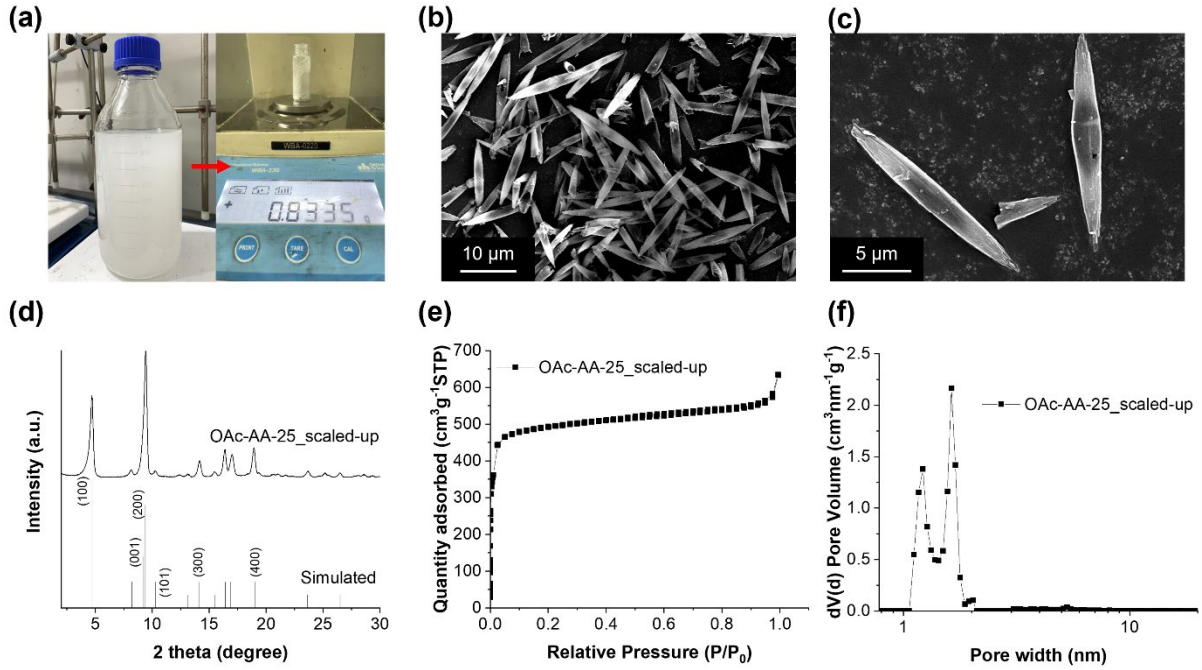

Fig. S5 Scale-up synthesis of OAc-AA-25. For scale-up synthesis, the OAc-AA-25 conditions were scaled up by a factor of 6 (a). SEM images of scaled up OAc-AA-25 (b, c) and corresponding XRD pattern (d), N_2 sorption isotherm at 77 K (e), and pore size distribution (f).

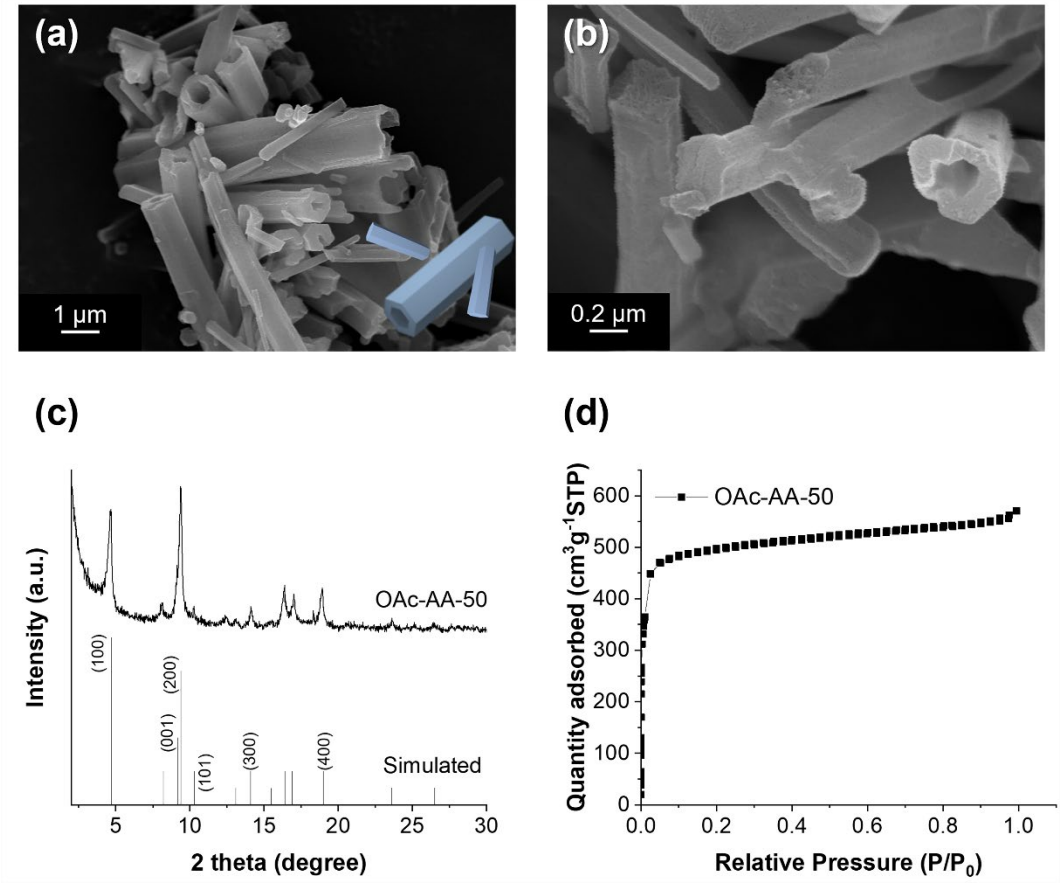

Fig. S6 SEM image (a, b) of OAc-AA-50, corresponding XRD pattern (c) and N_2 sorption isotherm at 77 K (d).

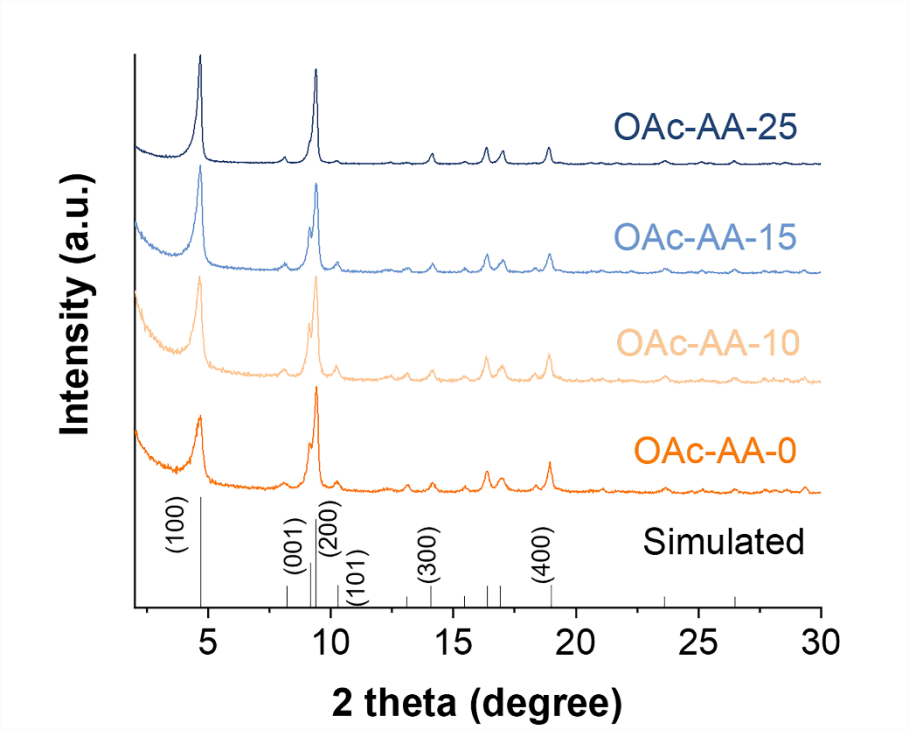

Fig. S7 XRD patterns of OAc-AA-*x*.

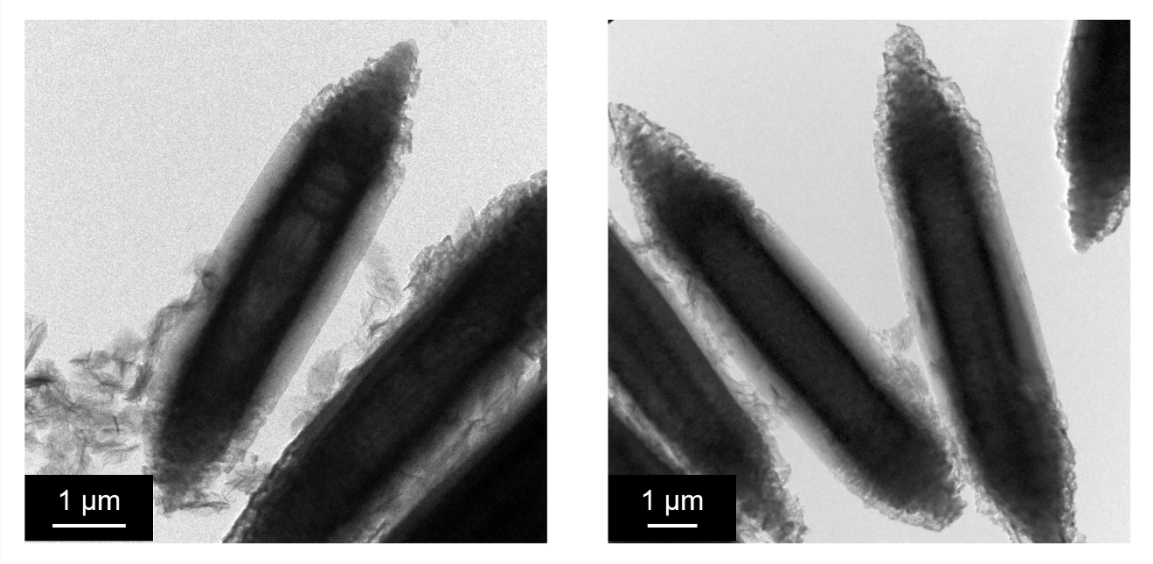

Fig. S8 TEM images of OAc-AA-25 in 10 seconds.

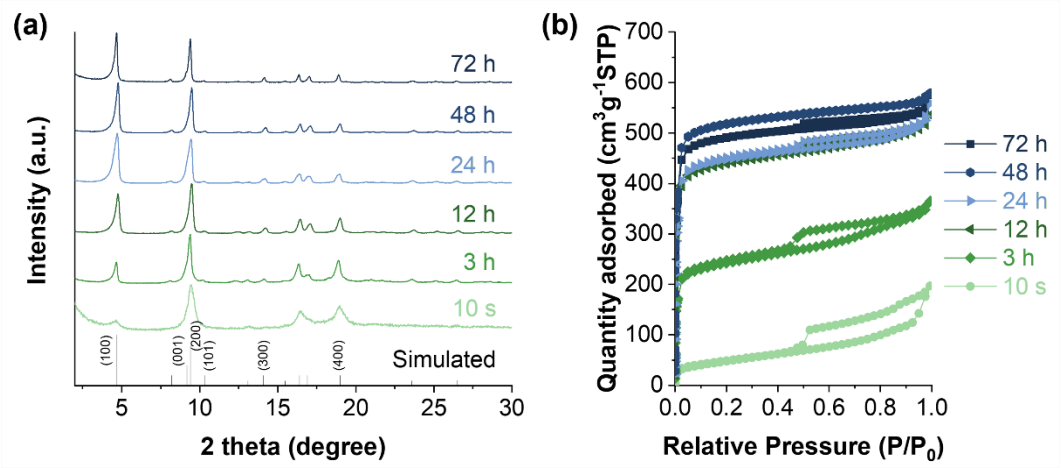

Fig. S9 XRD patterns (a) and N_2 sorption isotherms at 77 K (b) of OAc-AA-25 collected at different time intervals.

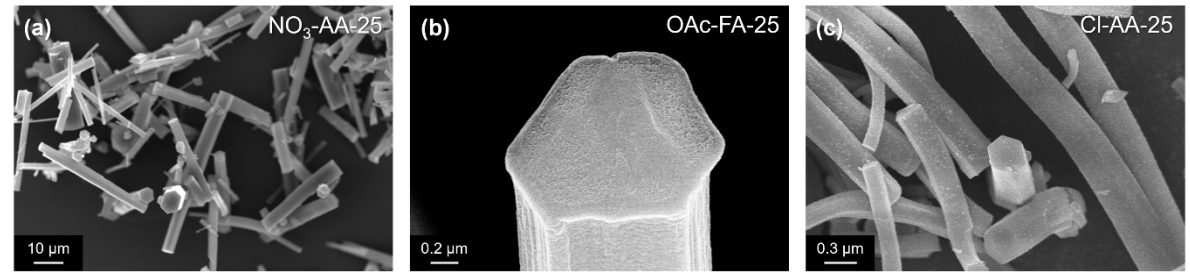

Fig. S10 SEM images of NO_3-AA-25 (a), OAc-FA-25 (b), and Cl-AA-25 (c).

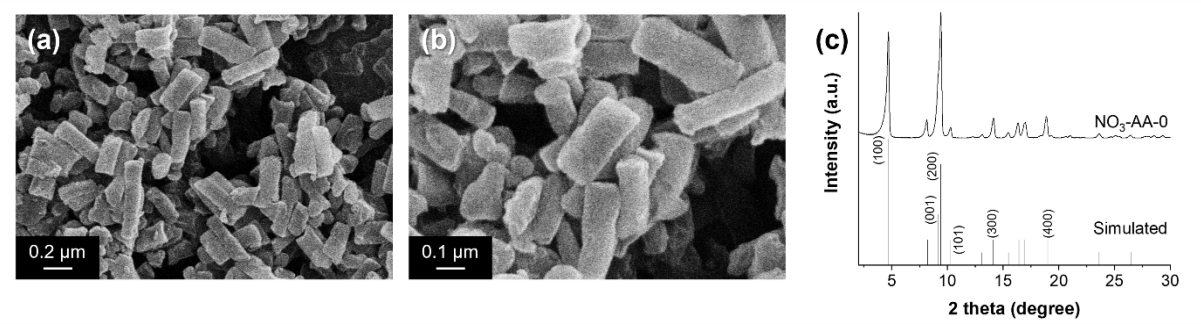

Fig. S11 SEM images at varying magnifications of NO_3-AA-0 (a, b) and corresponding XRD pattern (c).

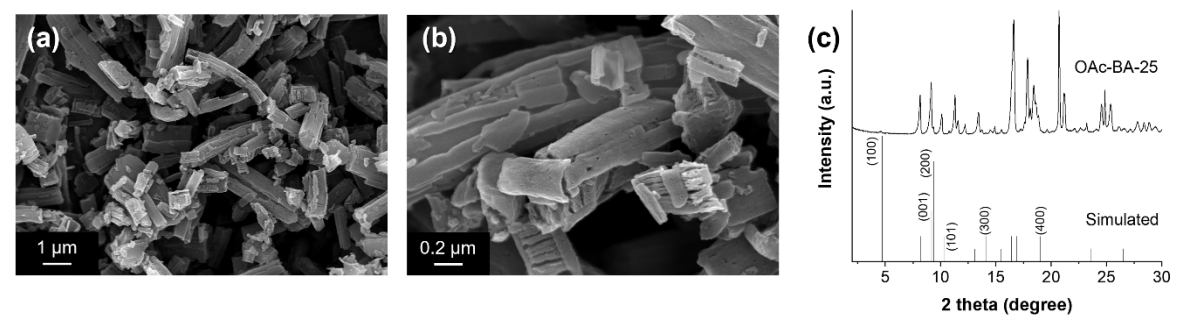

Fig. S12 SEM images at varying magnifications of OAc-BA-25 (a, b) and corresponding XRD pattern (c).

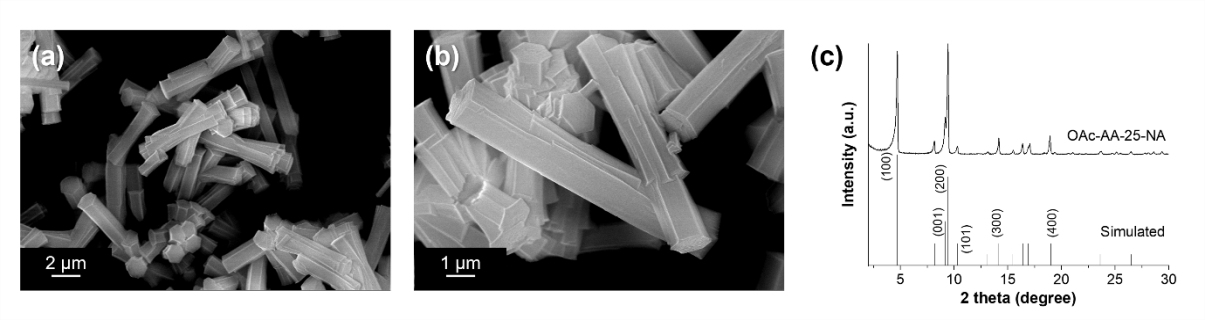

Fig. S13 SEM images at varying magnifications of OAc-AA-25-NA (a, b) and corresponding XRD pattern (c).

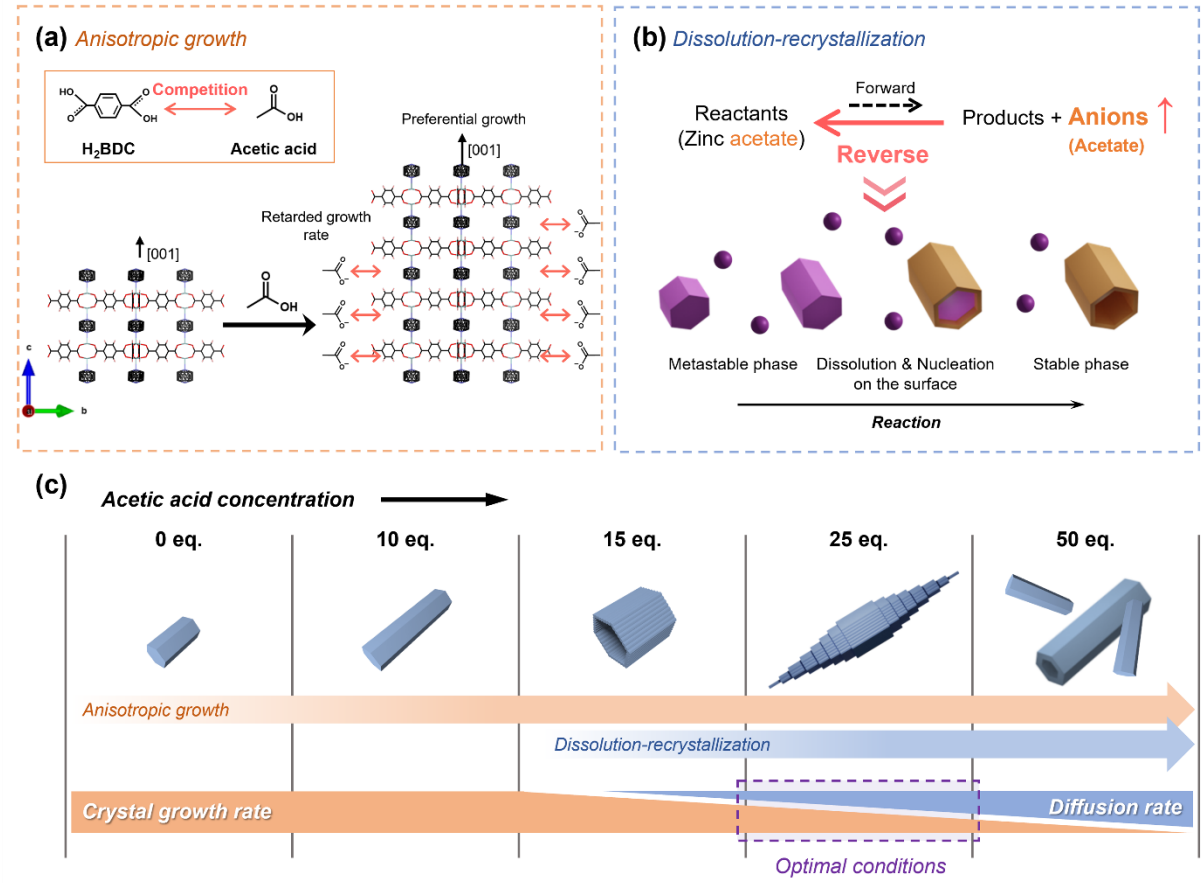

Fig. S14 Morphogenesis of ZnBD mediated by anisotropic growth (a) and dissolution-recrystallization (b), and the optimal conditions for the formation of oriented hollow superstructures in conjugate acid–base pair (c).

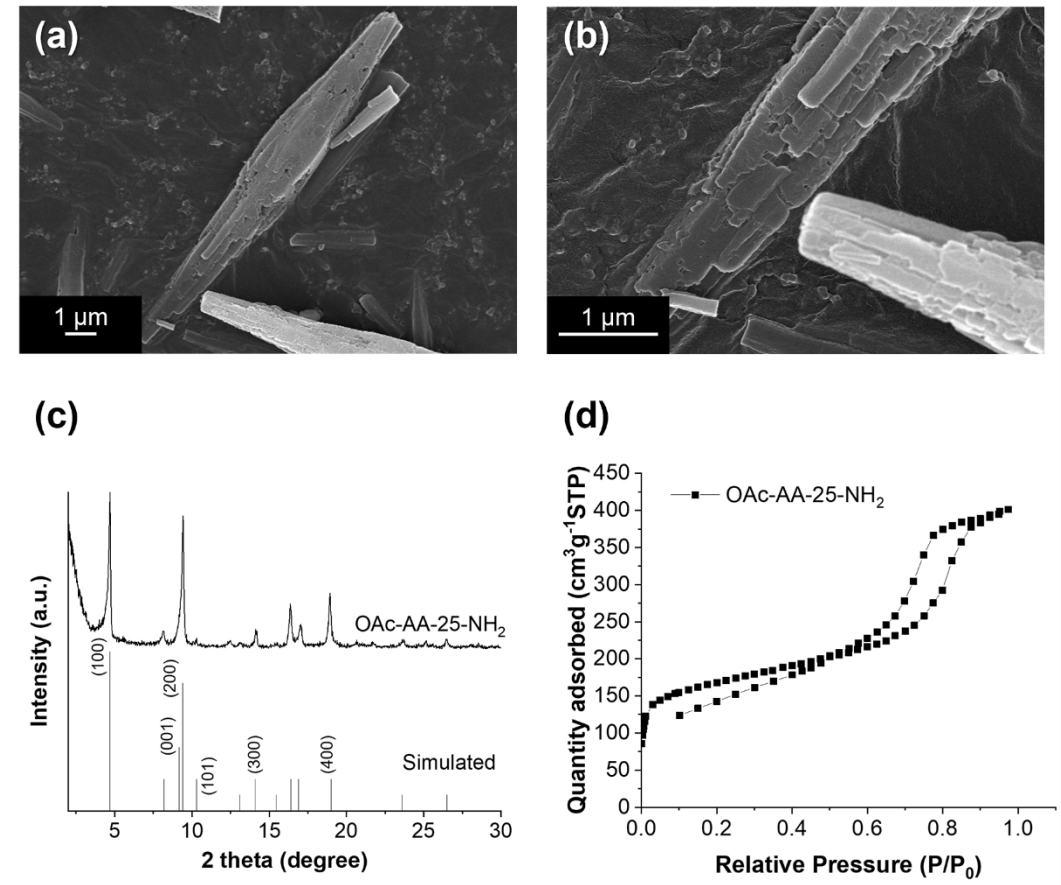

Fig. S15 SEM image of OAc-AA-25-NH_2 (a) corresponding XRD pattern (b) and N_2 sorption isotherm at 77 K (c).

We substituted the BDC ligand with 2-aminoterephthalic acid (ATA) ligand to synthesize $[Zn_2(ATA)_2DABCO]_n$ with oriented superstructure morphologies (denoted as OAc-AA-25-NH_2). In this system, a conjugate acid–base pair was generated in situ from zinc acetate and acetic acid at a 1:25 molar ratio prior to the introduction of the organic linkers. The resulting OAc-AA-25-NH_2 sample exhibits oriented superstructures constructed from arrays of anisotropic nanorods. Powder XRD patterns and N_2 adsorption isotherms confirm the high crystallinity and permanent porosity of OAc-AA-25-NH_2, with a BET surface area of 619 m^2 g^{-1}.

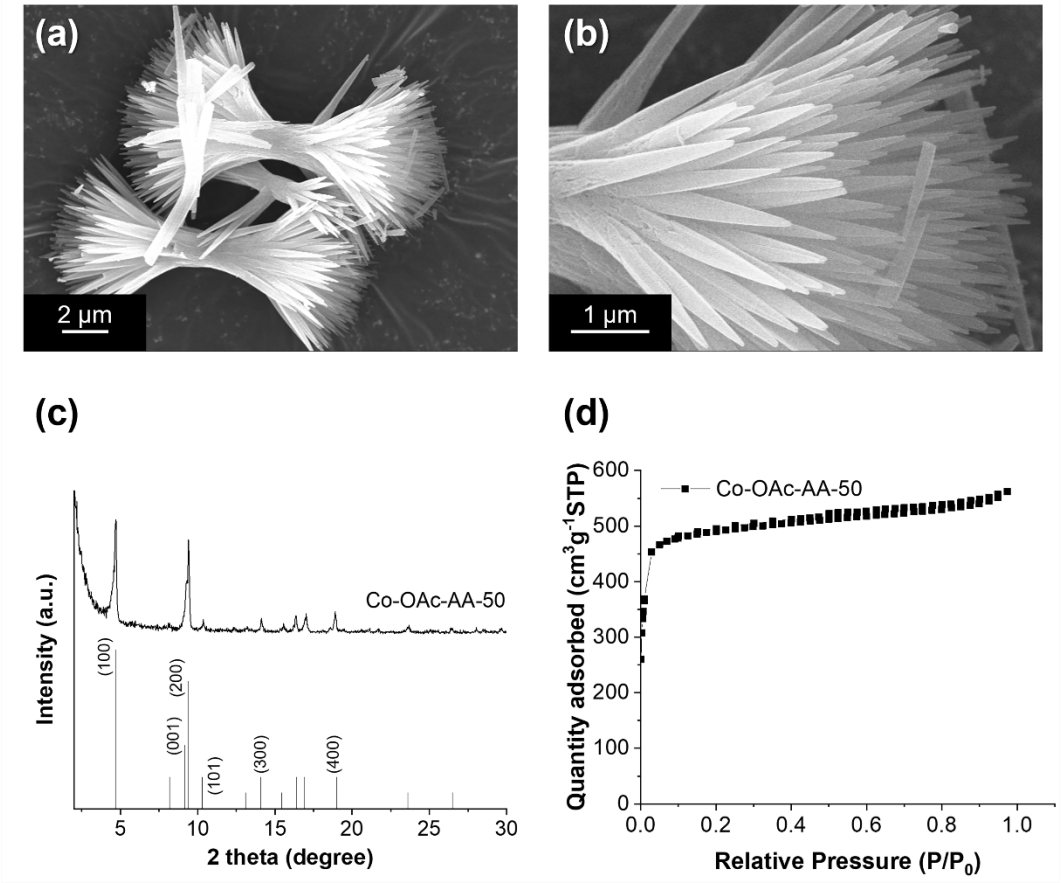

Fig. S16 SEM image of Co-OAc-AA-50 (a) corresponding XRD pattern (b) and N_2 sorption isotherm at 77 K (c).

We substituted the zinc acetate with cobalt acetate to synthesize $[Co_2(BDC)_2DABCO]_n$ with oriented superstructure morphologies (denoted as Co-OAc-AA-50). In this system, a conjugate acid–base pair was generated in situ from cobalt acetate and acetic acid at a 1:50 molar ratio prior to the introduction of the organic linkers. The resulting Co-OAc-AA-50 sample exhibits hierarchical superstructures constructed from anisotropic nanorods with low degree of orientation. Powder XRD patterns and N_2 adsorption isotherms confirm the high crystallinity and permanent porosity of Co-OAc-AA-50, with a BET surface area of 2015 $m^2\ g^{-1}$.

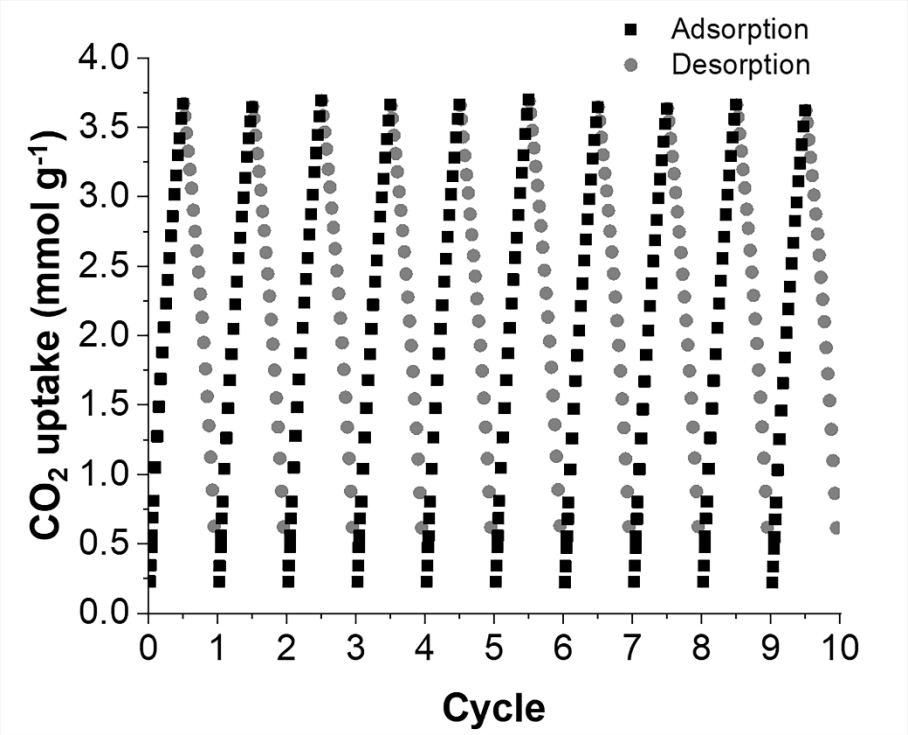

Fig. S17 Cyclic CO_2 adsorption–desorption performance of OAc-AA-25 for 10 cycles at 273 K.

Section 2. Supplementary Tables

Table S1. BET surface area, total pore volume of ZnBDs reported in this work and previous literature, determined by nitrogen physisorption.

	BET Surface Area (m^2g^{-1})	Total pore Volume[1] (cm^3g^{-1})	Ref.
OAc-AA-0	1401	0.731	This work
OAc-AA-10	1385	0.775	This work
OAc-AA-15	1598	0.799	This work
OAc-AA-25	2008	0.835	This work
OAc-AA-50	2021	0.854	This work
OAc-AA-25_scaled-up	2003	0.865	This work
ZBDh	1603	0.86	S1
Zn-rt	1911	0.71	S2
ZnBDh-D10	2160	-	S3
ZnBD-DMF	2104	0.8	S4

[1] Determined at P/P_0=0.95

Table S2. Production yield of S-A-x.

	Yield[1] (%)
OAc-AA-0	17
OAc-AA-10	62
OAc-AA-15	95
OAc-AA-25	93
OAc-AA-50	96
OAc-AA-25_scaled-up	80
NO_3-AA-0	4
NO_3-AA-25	5
OAc-FA-25	50
NO_3-NA-25	0
NO_3-FA-25	0
Cl-FA-25	0
Cl-AA-25	8
OFm-FA-25	0
OAc-BA-25	50

[1] Yield = actual yield/ theoretical yield * 100

Table S3. CO_2 uptake and CO_2/N_2 selectivity of OAc-AA-25 and OAc-AA-0 at 273 K.

	CO_2 uptake (0.15 bar)	CO_2 uptake (1 bar)	CO_2/N_2 selectivity[1] (15/85)
OAc-AA-25	0.850	3.799	19
OAc-AA-0	0.607	2.583	18

[1] Calculated by IAST; $S_{CO_2/N_2} = (x_{CO_2}/y_{CO_2})/(x_{N_2}/y_{N_2})$, x_i is the amount of each component in the adsorbed state and y_i is the molar fraction of each component in the gaseous state at equilibrium.

References

S1. H. Chun and J. Moon, *Inorg. Chem.*, 2007, **46**, 4371-4373.

S2. K. Zhou, S. Chaemchuen, Z. Wu and F. Verpoort, *Microporous Mesoporous Mater.*, 2017, **239**, 28-33.

S3. J. Hwang, R. Yan, M. Oschatz and B. V. K. J. Schmidt, *J. Mater. Chem. A*, 2018, **6**, 23521-23530.

S4. J. Hungerford and K. S. Walton, *Inorg. Chem.*, 2019, **58**, 7690-7697.